Fractal Analysis of Satellite-Detected Urban Heat Island Effect

Qihao Weng

Abstract

Surface radiant temperatures derived from Landsat TM thermal infrared images of 13 December, 1989, 03 March, 1996, and 29 August 1997 were used to study the urban heat island (UHI) phenomenon in Guangzhou, China. To examine the spatial distribution of surface radiant temperatures, transects were drawn and analyzed from each temperature image. Moreover, the fractal dimensions of these transects were computed using the divider method, so that the spatial variability of surface radiant temperatures caused by the thermal behavior of different land-cover types and landscape pattern characteristics can be better understood. The effect of urban development on the geographical distribution of surface radiant temperatures and thus on the UHI was also investigated. The results revealed two major heat islands, one in the southwest and the other in the east of the city. The areal extent of the UHIs varied as the season changed. The transact derived from the spring image had the lowest fractal dimension while that from the summer image the highest value. Urban development increased the spatial variability of radiant temperatures, resulting in higher fractal dimension values. The thermal surfaces have become more spatially uneven and the textures more complex.

Introduction

Urban development usually gives rise to a dramatic change of the Earth's surface, as natural vegetation is removed and replaced by non-evaporating and non-transpiring surfaces such as metal, asphalt, and concrete. This alteration will inevitably result in the redistribution of incoming solar radiation, and induce the urban-rural contrast in surface radiance and air temperatures. The difference in ambient air temperature between an urban area and its surrounding rural area is known as the effect of urban heat island (UHI). Given the relationship between air temperature, surface radiant temperature, and the texture of land cover, the impact of urban development on the UHI can be examined. Generally speaking, two types of UHI can be distinguished pertinent to the methods of temperature measurement: (1) the canopy layer heat island and (2) the boundary layer heat island (Oke, 1979). The former consists of air between the roughness elements, e.g., buildings and tree canopies, with an upper boundary just below roof level. The latter is situated above the former, with a lower boundary subject to the influence of the urban surface.

Studies on the UHI phenomenon using satellite remote sensing data have been conducted primarily using NOAA AVHRR data (Kidder and Wu, 1987; Balling and Brazell, 1988; Roth *et al.,* 1989; Gallo *et al.,* 1993). The 1.1-km spatial resolution of these data is found suitable only for small-scale urban temperature mapping. The 120-m spatial resolution Landsat TM thermal infrared (TIR) data have also been utilized to derive surface temperature. Carnahan and Larson (1990) and Larson and Carnahan (1997) used TM TIR data to observe meso-scale temperature differences between the urban area and the rural area in Indianapolis, Indiana. Kim (1992) studied the phenomenon of urban heat island in metropolitan Washington, D.C., and pinpointed the significance of soil albedo and moisture availability to surface energy balance. Nichol (1994) carried out a detailed study using TM thermal data to monitor microclimate for housing estates in Singapore. Weng (2001) examined the surface temperature pattern and its relationship with land cover in urban clusters in the Zhujiang Delta, China. More recently, researchers have used very high spatial resolution (10-m) ATLAS data (specifically, channel 13: 9.60 to 10.2 μm) to assess the UHI effect during daytime and nighttime in several cities and found it effective (Quattrochi and Ridd, 1994; Lo *et al.,* 1997; Quattrochi and Luvall, 1999). Quattrochi and Ridd (1998) applied 5-meter resolution TIMS (Thermal Infrared Multispectral Scanner) to study thermal energy responses for two broad classes (i.e., natural grass and urban/residential trees) and ten subclasses of vegetation in Salt Lake City, Utah. It is concluded that thermal responses for vegetation can be highly varied depending on the biophysical properties of the vegetation and other factors, and trees have a great effect on doming or mitigating the thermal radiation upwelling into the atmosphere. Satellite-derived surface temperatures are believed to correspond more closely with the canopy layer heat islands, although a precise transfer function between the ground surface temperature and the near ground air temperature is not yet available (Nichol, 1994). Byrne (1979) has observed a difference of as much as 20°C between the air temperature and the warmer surface temperature of dry ground.

Fractals have two basic characteristics suitable for modeling the topography and other spatial surfaces in the Earth's surface: self-similarity and randomness. Self-similarity refers to the well-known observation that the Earth's morphology appears similar across a range of scales (Malinverno, 1995). The concept of self-similarity also contains randomness, because the resemblance of the Earth's morphology at different scales is not exact but statistical (Malinverno, 1995). A fractal construction that includes randomness is termed a self-affine fractal. Self-affine fractals, such as fractional Brownian motion, requires rescaling

Department of Geography, Geology, and Anthropology, Indiana State University, Terre Haute, IN 47809 (geweng@scifac.indstate.edu).

Photogrammetric Engineering & Remote Sensing
Vol. 69, No. 5, May 2003, pp. 555–566.

0099-1112/03/6905–555$3.00/0

by different coordinates for an enlargement to look like the original, and have been used to model the topography of the Earth's surface (Mandelbrot, 1983). If remotely sensed imagery is considered to be one form of a spatial surface, then the complexity of the spatial surface should be apt for description and measurement by a fractal model (Lam, 1990), particularly by self-affine fractals. Surface radiant emittance, as recorded by thermal infrared sensors, includes both topographically and non-topographically induced high frequency variations such as roads and edges caused by different spectral characteristics of different neighboring land covers (Lam, 1990). The spatial surfaces generated from thermal infrared image data therefore have a fractal characteristic that mixes topographic and non-topographic frequencies. The use of fractals for analyzing thermal infrared images will improve our understanding of the thermal behavior of different land-cover types and the effect of landscape pattern on thermal environmental processes. The establishment of the relationships among land use, land cover, and radiant temperature makes it possible for a better scientific understanding of how the encroachment of urban and related uses on the natural environment have motivated the generation and growth pattern of UHIs. Moreover, because remote sensing analysis of UHIs often involve multiple sensors, it will be critical to know if fractal dimension is predictable with changes in spatial and spectral resolutions.

Previous studies have used fractals as a spatial measure for describing and analyzing remotely sensed imagery (De Cola, 1989; Lam, 1990; Emerson *et al.* 1999; Qiu *et al.* 1999). De Cola (1989) applied fractal analysis to describe the complexity of eight land-cover types in northwest Vermont, while Lam (1990) compared the fractal dimension of three land-cover types in the coastal Louisiana. Both studies employed Landsat TM images. Emerson *et al.* (1999) further studied the complexity of Normalized Difference Vegetation Index (NDVI) images derived from Landsat TM images, and examined the effect of changing pixel size on fractal dimension. Qiu and his team (Qiu *et al.,* 1999) used two AVIRIS (Airborne Visible Infra-Red Imaging Spectrometer) images of the Los Angeles area to compare the image complexity across the full spectral range of the hyperspectral images (224 bands). It was found that urban areas have higher fractal dimension values than rural areas, and the differences become more distinct in the visible bands. Most recently, Lam and her colleagues (Lam *et al.,* 2002) evaluated three fractal measures (i.e., isarithm, variogram, and a modified version of triangular prism), and compared them with Moran's I and Geary's C. It was concluded that both the isarithm and triangular prism methods could accurately measure a range of fractal surfaces, and that the variogram method was a relatively poor estimator particularly with high fractal dimension surfaces. In spite of these significant contributions, no substantial research has yet attempted to study a UHI pattern using fractal analysis, particularly to detect the temporal changes of the UHI pattern using multidate Landsat TM thermal infrared data. The objectives of this paper are (1) to detect and analyze the spatial patterns of urban heat islands derived from satellite imagery, (2) to examine the fractal characteristics of the urban heat island patterns, and (3) to model the UHI impact of urban development. While the focus of this study is to analyze satellite-detected UHI patterns, the results should also be of value for environmental management and urban planning within the study area.

The Study Area: Guangzhou, China

Guangzhou (also known as Canton) is located at latitude 23°08′ N and longitude 113°17′ E and lies at the confluence of two navigable rivers of the Zhujiang River (literally the "Pearl River") system (Figure 1). With a population of 3.99 million and total area of 1,444 km^2 (Guangdong Statistical Bureau, 1999), Guangzhou is the sixth most populous city in China. It has been the most important political, economic, and cultural center in southern China. The Guangzhou municipality comprises eight administrative districts in the city proper, and four rural counties (i.e., Huadu, Zengchen, Panyu, and Conghua). This study focuses on the city proper of Guangzhou.

Guangzhou has a history of urban development stretching across 2,000 years (Xu, 1990). It originated as a small village about 300 B.C. The city wall was first built in the third century, after China was united in the Qin Dynasty. During the Sui, Tang, and Song Dynasties, Guangzhou developed into the largest seaport in the nation as international sea going trade developed rapidly. With economic development and population increase, the city wall was expanded several times toward the east and the north. During the Qing Dynasty, the city was further expanded to the south, approaching the north bank of the Zhujiang. Following the establishment of the People's Republic of China in 1949, Guangzhou's locational advantages became more prominent, especially with the ending of the Vietnam conflict and the rising prosperity of Southeast Asia. Its urban development has progressed at an unprecedented pace since the implementation of the economic reforms after 1978, with eastward and northward expansion replacing the traditional southern and western expansion.

Data Acquisition and Processing

Computation of Surface Radiant Temperatures

The data used in this study were three Landsat Thematic Mapper (TM) images, dated on 13 December 1989, 03 March 1996, and 29 August 1997, respectively. Each Landsat image was rectified to a common UTM coordinate system based on 1:50,000-scale topographic maps. These data were resampled using the nearest-neighbor algorithm, with a pixel size of 30 m by 30 m for all bands including the thermal band. The resultant root-mean-squared error was found to be 0.77 pixel (23.1 m on the ground) for the 1989 image, and 0.58 pixel (17.4 m on the ground) for the 1996 and the 1997 images.

Surface radiant temperatures were derived from geometrically corrected TM thermal infrared data (band 6). The TM thermal band has a spatial resolution of 120 meters and a noise level equivalent to a temperature difference of 0.5°C (Gibbons and Wukelic, 1989). The local time of satellite overpass was in the morning (approximately 1000 hours), so that the chance for detecting a weak UHI is maximized. Because all the three images were acquired at approximately the same time, a comparative study is feasible. According to Professor Yang at South China Normal University, who has been studying the UHI of Guangzhou for decades using weather station and *in situ* data, air temperature difference between the urban and the rural peaks at 2100 hours, and goes down gradually until reaching a minimum at 1400 hours (Yang *et al.,* 1984). Although the impact of the diurnal heating cycle on the UHIs will be an interesting issue to address, there has been no attempt to include it here because TM does not provide day and night infrared images at the same day. Moreover, because absolute temperatures are not used for the purpose of computation, atmospheric correction was not carried out at this stage. A quadratic model was used to convert the digital

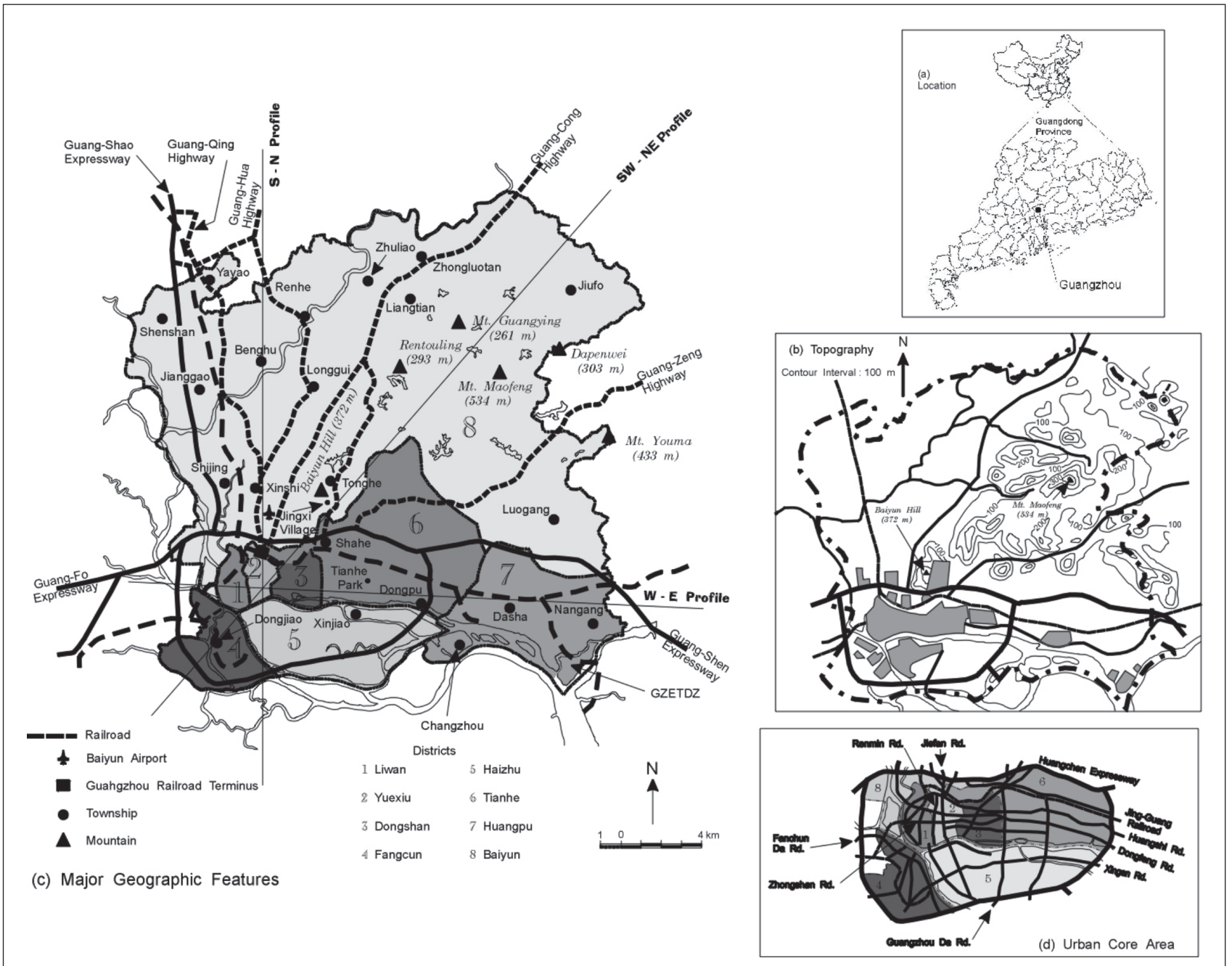

Figure 1. A map of the study area. The location, topography, and urban core area are shown as inset maps. W-E, S-N, and SW-NE profiles (transaction lines) for Figure 4 are indicated in (c).

number (DN) into radiant temperatures (Malaret *et al.,* 1985): i.e.,

$$T(k) = 209.831 + 0.834DN - 0.00133\ DN^2 \quad (1)$$

However, the temperature values obtained above are referenced to a black body. Therefore, corrections for emissivity (ε) became necessary according to the nature of land cover. Vegetated areas were given a value of 0.95 and non-vegetated areas 0.92 (Nichol, 1994). The emissivity corrected surface temperatures were computed as follows (Artis and Carnhan, 1982):

$$T_s = \frac{T(k)}{1 + (\lambda * T(k) / \rho)\ ln\varepsilon} \quad (2)$$

where λ is the wavelength of emitted radiance (for which the peak response and the average of the limiting wavelengths ($\lambda = 11.5\ \mu m$) (Markham and Barker, 1985) will be used), $\rho = h * c/\sigma$ ($1.438 * 10^{-2}$ mK), σ is the Stefan Bolzmann's constant ($5.67 * 10^{-8}$ W m^{-2} K^{-4} = $1.38 * 10^{-23}$ J/K), h is Planck's constant ($6.626 * 10^{(34}$ J sec), and c is the velocity of light ($2.998 * 10^8$ m/sec).

The normalized difference vegetation index (NDVI) image was computed for each year from visible (0.63 to 0.69 μm) and near-infrared (0.76 to 0.90 μm) data of TM images. The resultant NDVI image was thresholded into two categories to represent vegetated and non-vegetated areas. The thresholds were determined interactively by overlaying and comparing the NDVI images with false color composites. Equation 2 was then implemented with the aid of the Spatial Modeler algorithm in ERDAS Imagine.

Derivation of Land-Use and Land-Cover Data

Land-use and land-cover patterns for 1989, 1996, and 1997 were mapped using Landsat TM data. A modified version of the Anderson scheme of land-use/land-cover classification was adopted (Anderson *et al.,* 1976). The categories include (1) urban or built-up land, (2) barren land, (3) cropland (rice), (4) horticulture farms (primarily fruit trees), (5) dike-pond land, (6) forest, and (7) water.

At this stage, detection of fine changes in surface reflectances was required, and radiometric correction became necessary. Considering that no ancillary data on the atmospheric conditions during the satellite overpasses were available to account for atmospheric differences, a relative radiometric correction method using image regression (Jensen, 1996) was employed. The brightness value of each pixel of the subject scene (the 1989 and the 1996 scenes) was related to that of the reference image (the 1997 scene) band by band to produce a linear regression equation. This image normalization method can minimize or eliminate the effects caused by using historical remotely sensed images of non-anniversary dates (Jensen, 1996).

A supervised signature extraction with the maximum-likelihood algorithm was employed to classify the Landsat images. Both statistical and graphical analyses of feature selection were conducted. Bands 2 (green), 3 (red), and 4 (near infrared) were found to be most effective in discriminating each class, and were therefore used for classification. The feature selection process reduced the number of bands to be processed in the database, but should not affect the classification accuracy (Jensen, 1996). The accuracy of the classification was verified by field checking or by comparing with large-scale aerial photos and existing land-use and land-cover maps that have been field-checked. The urban and built-up lands were extracted from each land-use and land-cover image to create three urban maps.

The resultant land-use and land-cover maps for 1989, 1996, and 1997 are displayed in Plate 1. The overall accuracy of classification was determined to be 90.57 percent, 87.96 percent, and 85.43 percent, respectively. From these maps, it is clear that there have been considerable changes

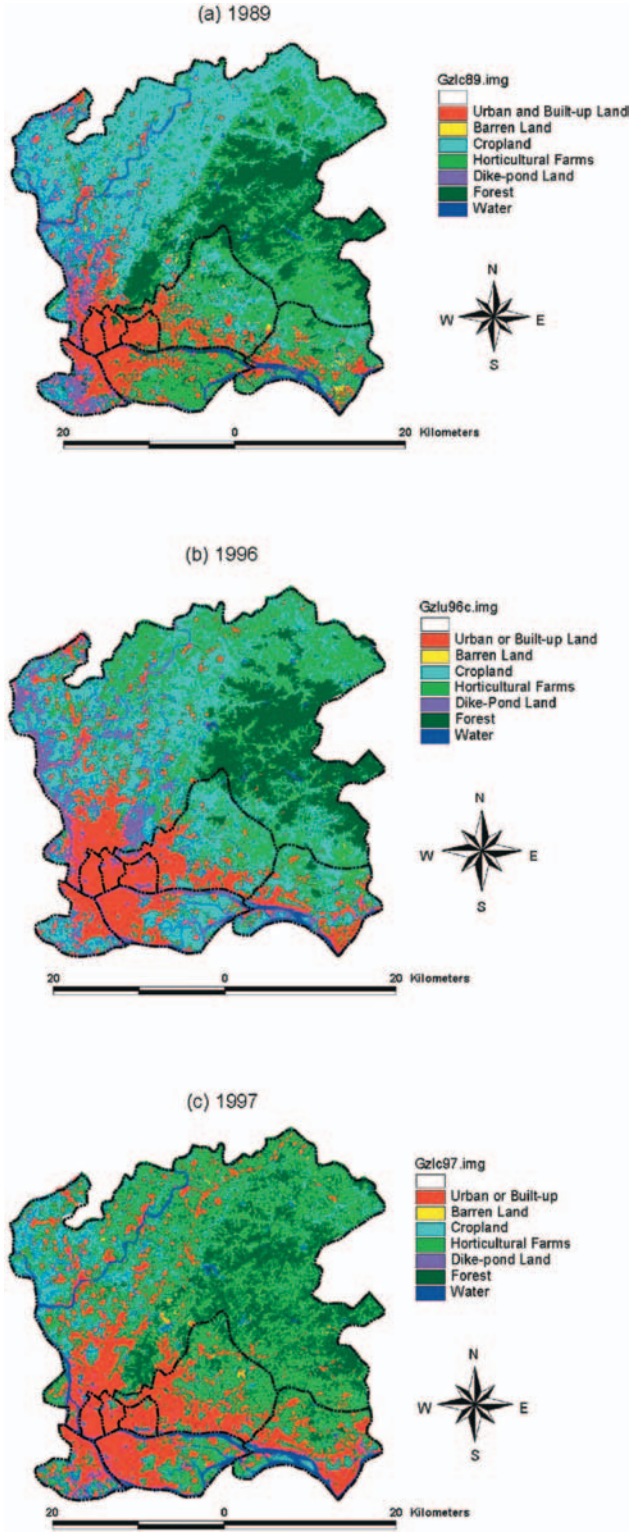

Plate 1. Land-use and land-cover maps for 1989, 1996, and 1997. The boundary of districts is superimposed.

in land use and land cover in Guangzhou during the 8-year period. The urban and built-up area was 194.8 km^2 in 1989 and 295.2 km^2 in 1997, indicating an increase of 100.4 km^2 (by 51.5 percent).

Data Analysis

Urban Heat Island Detection and Analysis

To examine the spatial distribution of surface radiant temperatures, each surface radiant temperature image was reclassified into four temperature zones based on the classification scheme of standard deviation (Smith, 1986). Four classes were differentiated based on the mean and standard deviation of the data distribution. Class one data are more than one standard deviation below the mean, class two values fall between the mean and one standard deviation below the mean, and so forth. The high and low temperature zones in each year were thus identified.

Based on the spatial patterns of radiant temperatures, three profiles (Figure 1b) were drawn to analyze the distribution of the urban heat islands. The west-east profile starts with the city's western boundary, from the Zhujiang (the Pearl River), through the Liwan, Yuexiu, Dongshan, and Tianhe Districts, and ends at the Nangang Township of the Huangpu District. The line basically goes along Zhongshan Road in the urban core area, and passes Tianhe Park and other rural areas in the suburb. Because the eastward expansion has been the main direction of urban development after the 1980s, an analysis of surface radiant temperature along the west-east profile is conducive to the examination of urban growth's impact on the thermal behavior of the environment.

The south-north profile sets out at the Fangcun District, passes through the Haizhu and Yuexiu Districts, and arrives at the Renhe Township of the Baiyun District. This line matches Jiefan Road in Yuexiu District, and also passes through the industrial area in the Haizhu District, Baiyun International Airport, and the newly developed areas around Xinshi Township. Therefore, an inquiry into this profile improves our understanding of how industrial development and infrastructure construction have altered the city's thermal characteristics.

The southwest-northeast profile begins at the Fangcun District. After successively passing through the Liwan, Yuexiu, and Tianhe Districts, it ends at the Jiufo Township of the Baiyun District. On the way to Jiufo, the profile also meets with Baiyun Hill, as well as a rapidly urbanized suburb at the base of Baiyun Hill, namely, Jinxi Village. Because it crosses over both the urban core area and the vast rural area in the northwestern part of the city, this profile contributes to our understanding of the urban-rural thermal difference.

Because the profiles cross the Pearl River, some ideas of the thermal difference between water bodies and terrestrial systems may be obtained.

Estimating the Fractal Dimension of Profiles

The fractal dimension of the spatial surfaces and profiles of remotely sensed data may be estimated using one of four main methods: (1) the box-counting method, (2) the spectral method, (3) the divider method, and (4) the triangular prism method. The box-counting method is implemented by laying a regular grid of boxes of characteristic size over the profile and counting the number of boxes intersected by the profile. The process is repeated for different sizes of box, and the number of boxes filled is plotted against the total number of boxes in the grid in a log-log form. If linear, the slope of this curve is related to the fractal dimension. The spectral method is based on the power spectrum.

The power spectrum of a series of elevation measurements quantifies how its overall variance is partitioned in a corresponding series of harmonic components whose wavelength varies between the length of a profile and twice the sampling interval (Priestly, 1981). The divider method (used in this paper), also known as ruler or compass method, is implemented by using different "step sizes" that represent the segments necessary to traverse a curve. For a comprehensive review of fractals, two texts on fractals (Mandelbrot, 1983; Feber, 1988) and review articles in the field of Earth sciences (Brown, 1995; Malinverno, 1995) are recommended.

The triangular prism method has also been used to calculate fractal dimensions of remotely sensed imagery (Clarke, 1986; Jaggi *et al.*1993; Qiu *et al.*1999). This method calculates the surface areas, defined by triangular prisms, using various sizes of measuring grids or cells. The four corners of each grid or cell on an image surface are denoted by pixel values of the four adjacent pixels. Each pixel value is interpreted as a "z" value in creating a three-dimensional cube. Assigning the mean value of the four pixels as its "z" value would generate the vertical line in the center of the cell. This creates a prism with four triangular facets. The surface area of this particular cell is obtained by summing those of the four triangular facets based on the trigonometric formula (Jaggi *et al.*1993).

With the divider method, the total length of a curve (α) is plotted against the step size (r) in a log-log form, and the fractal dimension D can be estimated from the slope of the resulting curve (B): i.e.,

$$\text{Log } \alpha = C + B * \log r \tag{3}$$

$$D = 1 - B \tag{4}$$

Figure 2 illustrates a self-affine fractal with a nominal length λ_0 digitized at discrete intervals of r and a standard

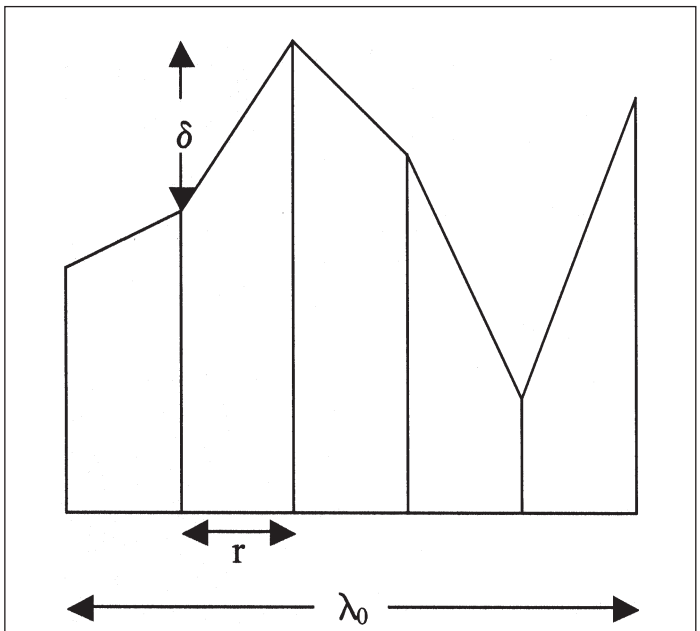

Figure 2. Estimation of fractal dimension using the divider method. In the figure, δ is the standard deviation of surface height (average deviation from the mean) over a length scale r, and λ_0 is the total profile length (Brown, 1995).

deviation of heights equal to δ. Then the total length of line α as a function of r is approximately

$$\alpha = \frac{\lambda_0}{r}\left(r^2 + \delta^2\right)^{1/2}. \quad (5)$$

For a self-affine fractal over distance r, the standard deviation of heights is

$$\delta = b\left(\frac{r}{b}\right)^{2-D} \quad (6)$$

where b is the crossover length. It is interpreted as the horizontal sampling interval, above which the divider method breaks down. To obtain a meaningful result from the divider method, data must be digitized at a scale much smaller than the crossover length (Brown, 1995). Replace δ with the above expression; then Equation 5 becomes

$$\alpha = \lambda_0\left[1 + \left(\frac{r}{b}\right)^{2(1-D)}\right]^{1/2}. \quad (7)$$

For $r \ll b$, log (α) versus log (r) has slope of $1 - D$. When $r \gg b$, then $\alpha \approx \lambda_0$. In this case, calculating D by using the slope of the r-α curve gives $D \approx 1$.

The algorithm used in this study was originally developed by Goodchild (1980) and Shelberg *et al.*(1983), and elaborated in Lam (1990), Lam and De Cola (1993), and Jaggi *et al.* (1993). This algorithm measures the fractal dimension of isarithm lines characterizing a spatial surface, and averages the D values of all lines as the surface's final fractal dimension. The isarithm lines of a remotely sensed image are generated by dividing the range of the pixel values of the image into equally spaced intervals. The length of each isarithm, as represented by the number of edges, is then measured at various step sizes. The logarithm of the number of edges is regressed against the logarithm of the step sizes. The slope of the regression is obtained using a best-fit linear model, and thus a D value for the isarithm. A computer program was written for implementing the procedure.

Modeling Urban Development Impact on the UHI

Given the relationship between surface radiant temperature and the texture of land cover that is influenced by land use, changes in land use and land cover (e.g., urban development) can have a profound effect on the surface radiant temperature and the UHI. The thermal signature of each land-cover type was obtained by overlaying a surface radiant temperature (T_s) image with a land-use and land-cover map in the same year. A mean temperature value (T_m) was then calculated for each land-cover type by averaging the T_s values of the three years. Next, the land-use and land-cover maps were converted into the maps of simulated radiant emittance by assigning T_m values to each land-cover class. Three profiles (W-E, S-N, and SW-NE) were drawn over these simulated maps, and the fractal dimensions of the profiles were calculated. By comparing the fractal dimension values in 1989, 1996, and 1997, one can see the impact of land use and land cover changes in general and urban development in particular on the growth patterns of the UHI.

Results

Spatial Patterns of the Urban Heat Islands

The statistics of surface radiant temperatures of each image by year are summarized in Table 1. On 13 December 1989, the lowest radiant temperature was 16.98°C, the highest temperature was 25.23°C, and the mean was 21.17°C, with a standard deviation of 1.72°C. A choropleth map (Figure 3) was produced to show the spatial distribution of the surface radiant temperatures based on the classification scheme of standard deviation. It is clear from the map that all the urban or built-up areas have a relatively high temperature, ranging from 21.17°C So 25.23°C. Some hot spots, or urban heat islands, could be identified. The most extensive UHI was distributed in the western part of the Haizhu District, an industrial region in the city. Another noticeable UHI was detected in the southeast corner of the city proper, where the Guangzhou Economical and Technological Development Zone (GETDZ) is located. Numerous factories have found their homes here after 1978, when the Chinese government initiated a series of preferential policies to special regions in order to attract foreign investment. There were also many small UHIs throughout the Tianhe District, which are related to the sparsely distributed industries in the region. However, there did not exist an extensive UHI in the old urban areas such as Liwan, Yuexiu, and Dongshan Districts, in spite of their high construction density. Apparently, commercial and residential areas are less effective in promoting the development of UHI.

The lowest temperature class (16.98 to 19.45°C) appeared in the following three areas: (1) the eastern part of Baiyun District around Maofeng Mountain; (2) Baiyun Hill, and (3) the southeastern part of Haizhu District. These areas were substantially rural at one time, and mostly covered by forest. Both the northwest Baiyun District and the west Fangcun District have a moderate temperature ranging from 19.45°C to 21.17°C, where cropland and dike-pond land prevailed.

TABLE 1. SUMMARY STATISTICS OF THE SURFACE RADIANT TEMPERATURES (UNIT: °C)

Date	Specification	Mean	Minimum	Maximum	Range	Standard Deviation	Coefficient of Variation
13 Dec 1989	Overall TM Scene	21.17	16.98	25.23	8.25	1.72	0.08
	W-E Profile	22.39	18.01	25.23	7.22	1.36	0.06
	S-N Profile	21.61	17.67	25.23	7.56	1.26	0.06
	SW-NE Profile	20.88	16.98	25.23	8.24	1.93	0.09
03 Mar 1996	Overall TM Scene	23.12	11.38	34.03	22.65	1.64	0.07
	W-E Profile	23.84	15.49	30.09	14.60	1.29	0.05
	S-N Profile	23.88	18.35	27.54	9.19	1.19	0.05
	SW-NE Profile	22.51	18.80	27.02	8.22	1.60	0.07
29 Aug 1997	Overall TM Scene	31.93	27.62	39.62	12.00	2.54	0.08
	W-E Profile	34.22	28.80	39.17	10.56	2.34	0.07
	S-N Profile	33.57	28.11	38.26	10.15	2.83	0.08
	SW-NE Profile	31.20	27.12	37.80	10.68	2.83	0.09

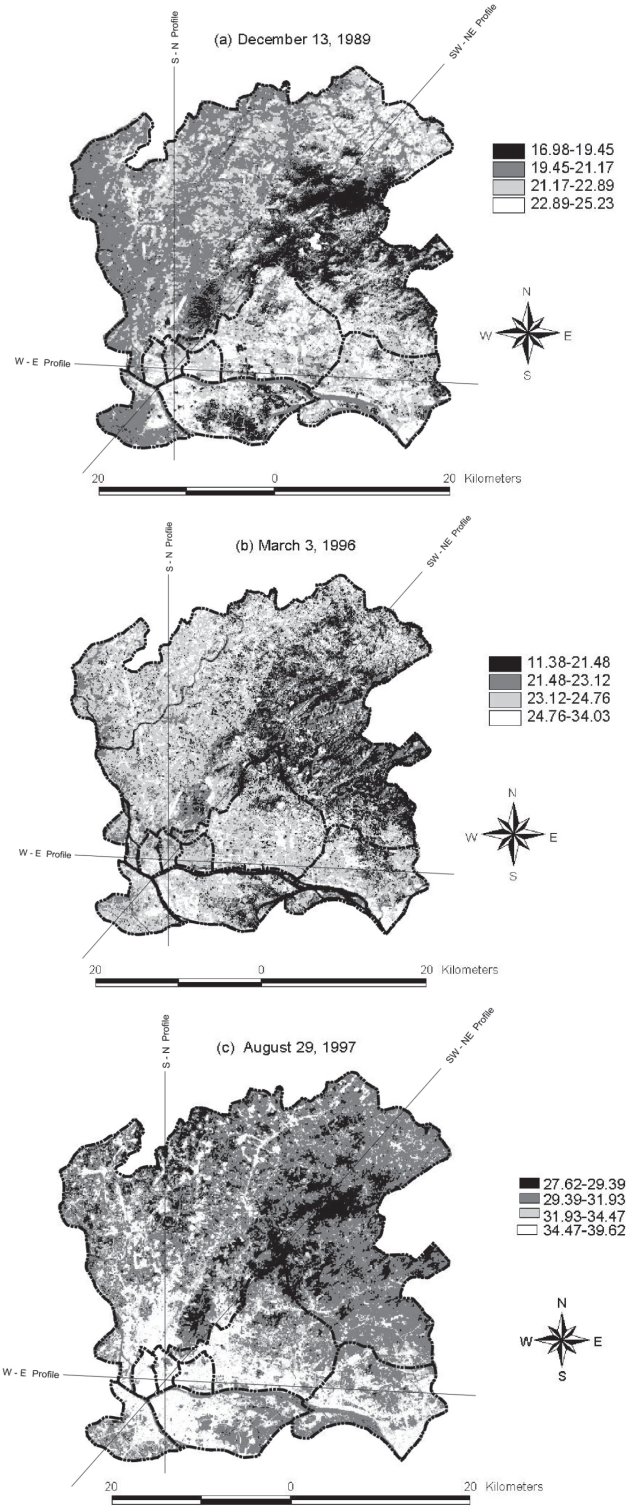

Figure 3. Spatial distribution of surface radiant temperature in 1989, 1996, and 1997. The boundary of districts is superimposed. W-E, S-N, and SW-NE profiles (transaction lines) for Figure 4 are indicated.

The spatial patterns of surface radiant temperature on 03 March 1996 were markedly different from those of 13 December 1989, as seen from Figure 3. These differences reflected not only the differences in solar illumination, the state of vegetation, and atmospheric influences of remotely sensed TM data set, but also changes in land use and land cover. The distinctive thermal characteristics of land-cover classes can affect the development of urban heat islands (Lo *et al.,* 1997; Weng, 2001). The mean radiant temperature of 03 March 1996 was 23.12°C, with a standard deviation of 1.64°C. However, a much higher range was observed for the date (22.65°C), varying from 11.38°C (minimum) to 34.03°C (maximum). While some of the urban or built-up areas fell into the highest temperature class (24.76 to 34.03°C), many others exhibited a moderate temperature around the mean. This indicates that urban surfaces experienced a much wider variation in radiant temperature. The thermal difference between the urban and the rural areas had been widened, reaching at 10°C, as compared to approximately 4°C on 13 December 1989. These different patterns are primarily attributed to a seasonal variation in solar illumination and the state of vegetation. The 1989 image was taken near winter solstice while the 1996 image around the spring equinox. The difference in data acquisition season was also evidenced in the radiant temperatures of water bodies. The radiant temperature of water bodies was in the intermediate temperature Class 3 (19.45 to 21.17°C) in 1989, but in the lowest temperature Class 4 (11.38 to 21.48°C) in 1996.

There were noteworthy UHIs (Figure 3), including one at west Haizhu, one at GETDZ of Huangpu District, and several others in the Tianhe District. These heat islands, however, were not spread out as extensively as those in 1989. The most significant difference between the two maps is seen in the northwest part of the Baiyun District. Urban development along the northward highways, particularly along the Guangzhou-Huaxian Highway, had created several visible urban heat strips. The conversion of cropland to other uses (e.g., to horticulture farms and to dike-pond land) has also altered the spatial patterns of surface radiant temperature, because cropland registered a lower temperature (mean = 23.26°C) than horticultural farms (23.61°C) but higher than dike-pond land (22.63°C).

The 1997 image (29 August) was taken in the hottest month. The average temperature was 31.93°C, with a range between 27.62°C and 39.62°C. The standard deviation was also the largest (2.54°C) among the three years, indicating that the surfaces experienced a wider variation in radiant temperature. The urban and rural areas can easily be distinguished from Figure 3. The urban areas showed a high temperature of over 34.47°C, while the rural settlements a minimal temperature of 31.93°C. The UHI expanded eastward from the urban core areas of Liwan, Yuexiu, and Dongshan to Huangpu, forming a heat island corridor. The UHI to the south of the Pearl River seemed to stretch out from the western Haizhu to the Fangcun District. Two large UHIs emerged, one centered at the Guangzhou Railroad Station and Baiyun International Airport, and the other to the east of Baiyun Hill. Both areas had been under a rapid urban sprawl since the 1990s. In additions, numerous strip-shaped UHIs have developed along the Guangzhou-Huaxian, Guangzhou-Huandong, and Guangzhou-Conghua Highways. During the summer time, Baiyun Hill seemed to be the only place where urban residents can escape from the heat owing to its dense vegetated cover.

Fractal Characteristics of the uhi Patterns

Figure 4 displays the W-E, S-N, and SW-NE temperature profiles for each year. From the city's core urban area in the southwest outward, there exist numerous "peaks," "valleys," "plateaus," and "basins," indicating the heterogeneous nature of radiant temperature over the space. Factors such as the spatial pattern of different land-cover classes,

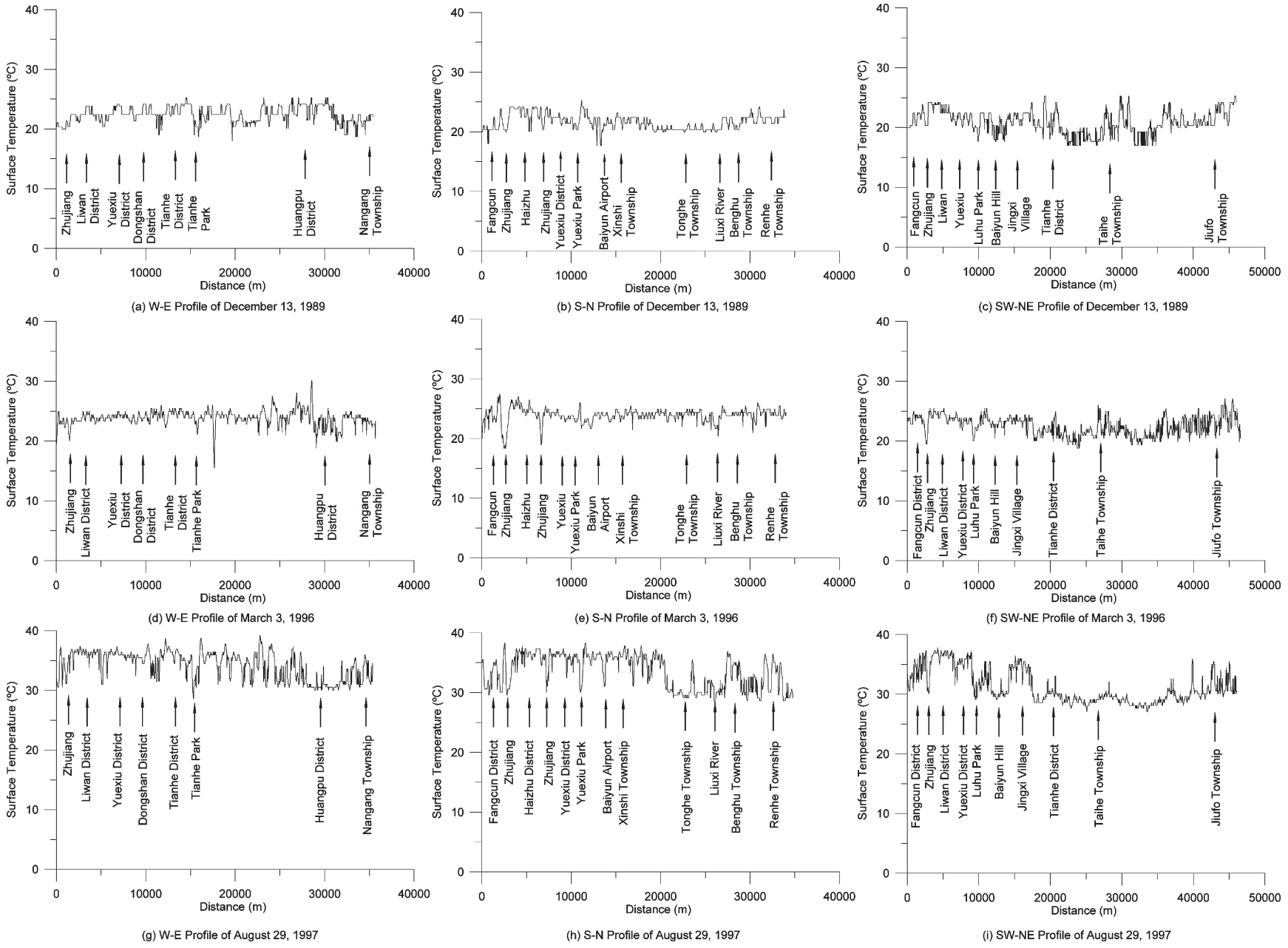

Figure 4. W-E, S-N, and SW-NE profiles across surface radiance temperature maps in Figure 3. Place names along the profiles are annotated in Figure 1b.

the occurrence of water bodies and parks, building and population densities, and the division of the city's functional districts, among many others, may have affected the development of UHIs. By visually comparing the profiles among the three rows of Figure 4, the seasonal variation of the UHI pattern becomes visible. Table 1 indicates that the mean value of surface radiant temperature varies from profile to profile. The W-E (1989 scene: 22.39°C; 1996 scene: 23.84°C; 1997 scene: 34.22°C) and S-N profiles (1989 scene: 21.61°C; 1996 scene: 23.88°C; 1997 scene: 33.57°C) generally have a higher value than the SW-NE profile (1989 scene: 20.88°C; 1996 scene: 22.51°C; 1997 scene: 31.20°C). This indicates that the W-E and S-N profiles cross more land cover types that possess higher thermal signatures (such as urban or built-up) than the SW-NE profile. Column 7 of Table 1 shows that the standard deviation value of surface radiant temperature varies from 1.19°C to 2.83°C among the nine profiles. Overall, the profiles of 03 March 1996 have the smallest standard deviation values (W-E profile: 1.29°C; S-N profile: 1.19°C; and SW-NE profile: 1.60°C), while those of 29 August 1997 have the highest values (W-E profile: 2.34°C; S-N profile: 2.83°C; and SW-NE profile: 2.83°C). It appears that the effect of UHI became more prominent as the season changes from spring to summer. The calculated values of fractal dimension with their corresponding coefficients of determination (*r*-squared, R^2) confirm this observation (Table 2). Spring possessed the lowest dimensions (W-E profile: 1.2327; S-N profile: 1.2088; and SW-NE profile: 1.3018), while summer possessed the highest dimensions (W-E profile: 1.4484; S-N profile: 1.5239; and SW-NE profile: 1.5219). Winter profiles exhibited a closer resemblance to spring rather than to summer, with a bit higher value of *D* than that of spring. (W-E profile: 1.2493; S-N profile: 1.2256; and SW-NE profile: 1.3716).

A comparison among the W-E, S-N, and SW-NE profiles indicates that the SW-NE profiles yield the highest average dimension (mean = 1.3984), followed by the S-N (mean = 1.3194) and W-E profiles (mean = 1.3103) (Table 2). This suggests that the SW-NE profiles are more spatially complex in texture than others. In other words, a higher spectral variability existed among the neighboring pixels because of topographic changes along the line (see Figure 1b) and the spatial arrangement and areal extent of different land-cover types. Indeed, the SW-NE profiles pass over all the seven land-cover types. Furthermore, a coefficient of variation (standard deviation/mean) is calculated, as an aspatial statistical measure, to indicate the data variability of surface radiant temperatures. The SW-NE profiles also possess the highest values, 0.09 for 1989, 0.07 for 1996, and 0.09 for 1997 (Table 1). This finding asserts that the spatial variability of surface radiant temperature along the SW-NE profile was the greatest (Figures 4c, 4f, and 4i). Table 1 shows that the temperature difference between the urban and the rural area along this transect may reach 8.22°C to 10.68°C, depending on the season.

The relatively low values of fractal dimension for the W-E profiles suggest that the texture is less spatially complex, i.e., the spectral responses to the thermal band along the line tend not to vary drastically (Figures 4a, 4d, and 4g). This is particularly true from the Zhujiang to the Tianhe District, where urban or built-up cover has occupied the majority of the surface. A computation of coefficients of variation indicates that the data variability of radiant temperatures is small in all the three years (0.06, 0.05, and 0.07, respectively). A closer look at Figure 4a, 4d, and 4g, however, reveals that it has a coarser texture from Tianhe Park eastward, where different types of land cover intermingle within a short distance.

The three S-N profiles were drawn to reveal different thermal responses among industrial, commercial, residential, airport, and rural areas. The resulting profiles for 13 December 1989 (Figure 4b) and for 03 March 1996 (Figure 4e) exhibit a smooth appearance, while the one for 29 August 1997 (Figure 4h) has many peaks and pits, especially in the northern part of Baiyun District. The fractal dimension values for these three profiles are 1.2256, 1.2088, and 1.5239, respectively, implying a fine texture for the winter and the spring profiles, but a coarse texture for the summer profile. However, water bodies such as the Zhujiang always create a "valley" regardless of the season, implying the importance of water bodies for damping the UHI effect. A careful examination of Figure 4h indicates that a "plateau" occurs extending from the Zhujiang to Xinshi Township. This "plateau" apparently corresponds to the south-north stretch of the UHI in the city, where residential, commercial, industrial, and infrastructure uses were predominant. Many newly developed areas in the northern part of Baiyun District in recent years have created a zone of "*kotadesasi*" (meaning the "town-village" mixed zones) (McGee, 1989). Whether the jig-jag appearance of the 1997 profile in this portion is caused by this pattern of urban development remains to be examined.

Urban Development and the Urban Heat Islands

In order to understand the impacts of land-use/land-cover change on surface radiant temperature, the characteristics of the thermal signatures of each land-cover type must be studied first. The average values of radiant temperatures by land-cover type are summarized in Table 3. It is clear that

TABLE 2. FRACTAL DIMENSION VALUE AND R^2 OF THE PROFILES

Date	Profile	Fractal Dimension	Coefficient of Determination
13 Dec 1989	W-E Profile	1.2493	0.8664
	S-N Profile	1.2256	0.8639
	SW-NE Profile	1.3716	0.9026
03 Mar 1996	W-E Profile	1.2327	0.8587
	S-N Profile	1.2088	0.8549
	SW-NE Profile	1.3018	0.8779
29 Aug 1997	W-E Profile	1.4484	0.9228
	S-N Profile	1.5239	0.9429
	SW-NE Profile	1.5219	0.9427
Mean	W-E Profile	1.3103	
	S-N Profile	1.3194	
	SW-NE Profile	1.3984	

TABLE 3. AVERAGE SURFACE RADIANT TEMPERATURE (°C) BY LAND-COVER TYPE

Land Cover	13 Dec 1989 (Standard Deviation)	03 Mar 1996 (Standard Deviation)	29 Aug 1997 (Standard Deviation)	Average
Urban or Built-Up Land	22.50 (1.23)	23.95 (1.30)	34.75 (2.09)	27.07
Barren Land	22.16 (1.33)	23.79 (1.38)	32.23 (2.05)	26.06
Cropland	21.30 (1.26)	23.26 (1.37)	30.96 (1.72)	25.17
Horticulture Farms	21.71 (1.83)	23.61 (1.52)	31.24 (1.90)	25.52
Dike-pond Land	20.18 (0.26)	22.63 (1.62)	32.83 (2.46)	25.21
Forest	19.77 (1.74)	21.82 (1.40)	29.88 (1.15)	23.82
Water	20.35 (0.72)	20.36 (1.98)	31.34 (1.45)	24.02

urban or built-up land exhibited the highest radiant temperature (22.50°C in 1989, 23.95°C in 1996, and 34.75°C in 1997), followed by barren land (22.16°C in 1989, 23.79°C in 1996, and 32.94°C in 1997). This implies that urban development does bring up radiant temperature by replacing natural vegetation with non-evaporating, non-transpiring surfaces such as stone, metal, and concrete. The standard deviations of the radiant temperature values were relatively small for urban cover, indicating that urban surfaces did not experience a wide variation in radiant temperature because of the dry nature of non-evapotransipirative materials. The lowest radiant temperature in 1989 was observed in forest (19.77°C), followed by dike-pond land (20.18°C) and water bodies (20.35°C). On 29 August 1997, the lowest radiant temperature was found in forest (29.88°C), followed by cropland (30.96°C) and horticultural farms (31.24°C). This pattern is in contrast with that in 1996, when the lowest radiant temperature was detected in water (20.36°C), followed by forest (21.82°C) and dike-pond land (22.63°C). This different pattern is primarily attributed to the seasonal differences in solar illumination, the state of vegetation, and atmospheric influences on the remotely sensed TM data set. Forests showed a considerably lower radiant temperature in all years, because dense vegetation can reduce the amount of heat stored in the soil and surface structures through transpiration. Water bodies tended to get warm slowly during the day owning to convection. Cropland and horticulture farms had an intermediate level of radiant temperature, because they consisted of sparse vegetation and exposed bare soil.

A mean temperature T_m value was calculated for all land-cover types by averaging the T_s values of the three years. The land-use and land-cover maps of 1989, 1996, and 1997 were converted into a map of mean temperature by assigning T_m values to each land-cover type. The fractal dimensions were calculated for the three profiles over these mean temperature maps. Results indicate that all the three profiles have increased their *D* value over the time (Table 4). The W-E profile increased from 1.1761 in 1989 to 1.1777 in 1996 and to 1.1922 in 1997; the S-N profile from 1.1921 to 1.1937 and 1.2093; and the SW-NE profile from 1.1902 to 1.1974 and 1.1984. The increase in *D* values implies that the thermal surfaces became more spatially uneven and the textures more complex due to the land-use and land-cover changes. Because the three profiles pass over both the urban and the rural areas, these results reflect well the impact of urban growth on the texture of thermal surfaces. Urban development has increased the variability of radiant temperatures over the space, resulting in higher fractal dimension values of the transects. Table 4 indicates that, among the three profiles, the largest amount of change in *D* value occurs in the S-N profile (0.0172), followed by the W-E profile (0.0161), and the SW-NE profile (0.0082).

TABLE 4. FRACTICAL DIMENSION VALUE AND R^2 FOR THE PROFILES OF SIMULATED TEMPERATURES

Year	Profile	Fractal Dimension	Coefficient of Determination
1989	W-E Profile	1.1761	0.8324
	S-N Profile	1.1921	0.8383
	SW-NE Profile	1.1902	0.8476
1996	W-E Profile	1.1777	0.8381
	S-N Profile	1.1937	0.8475
	SW-NE Profile	1.1974	0.8521
1997	W-E Profile	1.1922	0.8389
	S-N Profile	1.2093	0.8417
	SW-NE Profile	1.1984	0.8435

That is to say, land-use and land-cover changes, especially urban development, have caused a greater contrast in the surface thermal properties in the S-N and W-E directions. The scope of the UHI has extended to the north and to the east direction as a result of urban development.

Discussions and Conclusions

The utility of Landsat TM infrared data to detect urban heat islands in Guangzhou proved to be effective. Two major heat islands were detected, one in the west Haizhu District and one in the Guangzhou Economic and Technological Development Zone, and several others in the Tianhe District. The distribution of the UHIs was closely associated with industrial land uses but not with residential land uses. The areal extent of the UHIs varied as the season changed. The profiles derived from the spring image had the lowest fractal dimension while from the summer image the highest value. Changes in fractal dimension in different seasons were not only attributed to solar illumination and climatologic conditions relating to soil moisture and air temperature, but also to the topographic variation and the spatial arrangement and areal extent of different land cover types. Urban development increased the spatial variability of radiant temperatures, resulting in higher fractal dimension values. The thermal surfaces have become more spatially uneven and the textures more complex.

As has been pointed out by Lam (1990), the computation results of fractal dimension are subject to the influence of the method used. For the sake of simplicity, the divider method was used in this study. The divider methods give a correct *D* value for self-affine fractals only under certain conditions (Mandelbrot, 1983), but always give a good approximation for self-similar fractals. Further studies should compare this method with the box and spectral methods. The spectral method is expected to be valid for self-affine fractals in the form of time or spatial series (Brown, 1995). The box method is also able to give a reliable *D* value for self-affine fractals under certain circumstances. The triangular prism method can accurately measure a range of fractal surfaces, but is sensitive to contrast stretching (Lam *et al.,* 2002).

Many factors, such as solar illumination, the state of vegetation, atmospheric effect, land-use and land-cover pattern, and topography, affect the fractal dimensionality from remotely sensed imagery. More research is needed to differentiate the impact of each element. Radar generated topography data (e.g., SRTM, lidar, IFSAR) may be desirable to relate urban topography to UHI studies. Remotely sensed data from different sensors should be acquired to examine the effects of various spectral and spatial resolutions on the resultant fractal dimensions (Lam, 1990). For example, application of fractals to data from the NASA Earth Observation System sensors (e.g., Landsat 7, ASTER, MODIS) holds great potential for the analysis and characterization of urban thermal landscape, as well as for the planning and development of more advanced thermal infrared platforms.

It should also be noted that the computation of surface radiant temperature can be far more complicated than the method presented in the current study. Quattrochi and Goel (1995) conducted a comprehensive review on major technical and theoretical difficulties in using thermal-infrared remotely sensed data obtained at different spatial and temporal scales. Factors such as the scale-dependent nature of landscape characteristics, physiography, emissivity, atmospheric effects, and sensor-to-target noise have contributed to the difficulties in the determination of surface temperatures (Quattrochi and Goel, 1995). Radiant temper-

atures may be higher than surface temperatures. Goetz *et al.* (1993) found that Landsat 5 TM data consistently overestimated surface temperatures by 1°C to 8°C (compared with near-surface-level temperatures) due primarily to the sensor's radiometric characteristics. The effects of surface roughness on surface temperature have not been taken into account in this paper. Several authors (Kimes, 1983; Cassels *et al.,* 1992a; Cassels *et al.,* 1992b) have elaborated on this issue, and suggest scrutinizing the temperatures of each part of the vegetation-ground system and examining the effects of different canopy structures. Effective land surface temperature can be derived only after its relationship to the component temperatures have been mathematically modeled. In addition, a more complicated emissivity correction scheme should be applied. Effective measurement of surface temperatures requires the analysis of the significance of the nature of surface and its roughness on emissivity. The emissivity values for urban areas are highly variable, and need to be refined in future studies.

Acknowledgments

The funded support of the National Geographic Society (Grant number: 6811-00) is greatly acknowledged. The comments and suggestions of three anonymous reviewers helped improve this paper.

References

Anderson, J. R., E. E., Hardy, J. T., Roach, and R.E. Witmer, 1976. *A Land Use and Land Cover Classification Systems for Use with Remote Sensing Data,* USGS Professional Paper 964, U.S. Government Printing Office, Washington, D.C., 27 p.

Artis, D.A., and W.H. Carnahan, 1982. Survey of emissivity variability in thermography of urban areas, *Remote Sensing of Environment*, 12:313–329.

Balling, R.C., and S.W. Brazell, 1988. High resolution surface temperature patterns in a complex urban terrain, *Photogrammetric Engineering & Remote Sensing*, 54:1289–1293.

Brown, S.R., 1995. Measuring the dimension of self-affine fractals: examples of rough surfaces, *Fractals in the Earth Sciences* (C.C. Barton and P.R. LaPointe, editors), Plenum Press, New York, N.Y., pp. 77–87.

Byrne, G.F., 1979. Remotely sensed land cover temperature and soil water status — A brief review, *Remote Sensing of Environment*, 8:291–305.

Carnahan, W.H., and R.C. Larson, 1990. An analysis of an urban heat sink, *Remote Sensing of Environment*, 33:65–71.

Cassels, V., J.A. Sobrino, and C. Coll, 1992a. On the use of satellite thermal data for determining evapotranspiration in partially vegetated areas, *International Journal of Remote Sensing*, 13:2669–2682.

———, 1992b. A physical model for interpreting the land surface temperature obtained by remote sensors over incomplete canopies, *Remote Sensing of Environment*, 39:203–211.

Clarke, K.C., 1986. Computation of the fractal dimension of topographic surfaces using the triangular prism surface area method, *Computers and Geosciences*, 12(5):713-722.

De Cola, L., 1989. Fractal analysis of a classified Landsat scene, *Photogrammetric Engineering and Remote Sensing*, 55(5):601–610.

Emerson, C.W., N.S.N. Lam, and D.A. Quattrochi, 1999. Multiscale fractal analysis of image texture and pattern, *Photogrammetric Engineering & Remote Sensing*, 65(1):51–61.

Feder, J., 1988. *Fractals*, Plenum Press, New York, N.Y., 283 p.

Gallo, K.P., A.L. McNab, T.R. Karl, J.F. Brown, J.J. Hood, and J.D. Tarpley, 1993. The use of NOAA AVHRR data for assessment of the urban heat island effect, *Journal of Applied Meteorology*, 32:899–908.

Gibbons, D.E., and G.E. Wukelic, 1989. Application of Landsat Thematic Mapper data for coastal thermal plum analysis at Diablo Canyon, *Photogrammetric Engineering & Remote Sensing*, 55(6):903–909.

Goetz, S.J., F.G. Hall, B.L. Markham, and R.O. Dubayah, 1993. Inter-comparison of retrieved surface temperature from multi-resolution sensors at the FIFE site, *Technical Papers of ASPRS/ACSM 1993*, 16–18 February, New Orleans, Louisiana, pp. 108–117.

Goodchild, M.F., 1980. Fractals and the accuracy of geographical measures, *Journal of Mathematical Geology*, 12(2):85–98.

Guangdong Statistical Bureau, 1999. *Guangdong Statistical Yearbook*, China Statistical Press, Beijing, China, 721 p. (in Chinese).

Jaggi, S., D. Quattrochi, and N.S. Lam, 1993. Implementation of operation of three fractal measurement algorithms for analysis of remote sensing data, *Computers & Geosciences*, 19(6): 745–767.

Jensen, J.R., 1996. *Introductory Digital Image Processing: A Remote Sensing Perspective, Second Edition*, Prentice Hall, Upper Saddle River, New Jersey, 316 p.

Kidder, S.Q., and H.T. Wu, 1987. A multispectral study of the St. Louis area under snow-covered conditions using NOAA-7 AVHRR data, *Remote Sensing of Environment*, 22:159–172.

Kim, H.H., 1992. Urban heat island, *International Journal of Remote Sensing,* 13(12):2319–2336.

Kimes, D.J., 1983. Remote sensing of row crop structure and component temperatures using directional radiometric temperatures and inversion techniques, *Remote Sensing of Environment*, 13:33–55.

Lam, N.S.N., 1990. Description and measurement of Landsat TM images using fractals, *Photogrammetric Engineering & Remote Sensing*, 56(2):187–195.

Lam, N.S.N., and L. De Cola, 1993. *Fractals in Geography*, Prentice Hall, Englewood Cliffs, New Jersey, 308 p.

Lam, N.S.N., H. Qiu, D.A. Quattrochi, and C.W. Emerson, 2002. An evaluation of fractal methods for characterizing image complexity, *Cartography and Geographic Information Science*, 29(1):25–35.

Larson, R.C., and W.H. Carnahan, 1997. The influence of surface characteristics on urban radiant temperatures, *Geocarto International*, 12(3):5–16.

Lo, C.P., D.A. Quattrochi, and J.C. Luvall, 1997. Application of high-resolution thermal infrared remote sensing and GIS to assess the urban heat island effect, *International Journal of Remote Sensing,* 18:287–304.

Malaret, E., L.A. Bartolucci, D.F. Lozano, P.E. Anuta, and C.D. McGillem, 1985. Landsat-4 and Landsat-5 Thematic Mapper data quality analysis, *Photogrammetric Engineering & Remote Sensing*, 51:1407–1416.

Malinverno, A., 1995. Fractals and ocean floor topography: A review and a model, *Fractals in the Earth Sciences* (C.C. Barton and P.R. LaPointe, editors), Plenum Press, New York, N.Y., pp. 107–130.

Mandelbrot, B.B., 1983. *The Fractal Geometry of Nature*, W.H. Freeman, San Francisco, California, 468 p.

Markham, B.L., and J.K. Barker, 1985. Spectral characteristics of the LANDSAT Thematic Mapper sensors, *International Journal of Remote Sensing*, 6:697–716.

McGee, T.G., 1989. Urbanisasi or kotadesasi? Evolving patterns of urbanization in Asia, *Urbanization in Asia: Spatial Dimensions and Policy Issues* (F. Coasta, A.K. Dutt, L.J.C. Ma and A.G. Nobel, editors), University of Hawaii Press, Honolulu, Hawaii, pp. 93–108.

Nichol, J.E., 1994. A GIS-based approach to microclimate monitoring in Singapore's high-rise housing estates, *Photogrammetric Engineering & Remote Sensing*, 60:1225–1232.

Oke, T.R., 1979. *Technical Note No. 169: Review of Urban Climatology*, World Meteorological Organization, Geneva, Switzerland, 43 p.

Priestly, M.B., 1981. *Spectral Analysis and Time Series*, Academic Press, London, United Kingdom, 890 p.

Qiu, H.L., N.S.N. Lam, D.A. Quattrochi, and J.A. Gamon, 1999. Fractal characterization of hyperspectral imagery, *Photogrammetric Engineering & Remote Sensing*, 65(1):63–71.

Quattrochi, D.A., and N.S. Goel, 1995. Spatial and temporal scaling of thermal remote sensing data, *Remote Sensing Review*, 12:255–286.

Quattrochi, D.A., and J.C. Luvall, 1999. *High Spatial Resolution Airborne Multispectral Thermal Infrared Data to Support Analysis and Modeling Tasks in the EOS IDS Project ATLANTA*, URL: http://wwwghcc.msfc.nasa.gov/atlanta/, Global Hydrology and Climate Center, NASA, Huntsville, Alabama (date last accessed: 19 September 2002).

Quattrochi, D.A., and M.K. Ridd, 1994. Measurement and analysis of thermal energy responses from discrete urban surfaces using remote sensing data, *International Journal of Remote Sensing*, 15(10):1991–2022.

———, 1998. Analysis of vegetation within a semi-arid urban environment using high spatial resolution airborne thermal infrared remote sensing data, *Atmospheric Environment*, 32(1):19–33.

Roth, M., T.R. Oke, and W.J. Emery, 1989. Satellite derived urban heat islands from three coastal cities and the utilisation of such data in urban climatology, *International Journal of Remote Sensing*, 10:1699–1720.

Shelberg, M.C., N.S.N. Lam, and H. Moellering, 1983. Measuring the fractal dimensions of surfaces, *Proceedings of the Sixth International Symposium on Automated Cartography (Auto-Carto 6)*, 04–06 October, Ottawa, Canada, 2:319–328.

Smith, R.M., 1986. Comparing traditional methods for selecting class intervals on choropleth maps, *Professional Geographer*, 38(1):62–67.

Weng, Q., 2001. A remote sensing-GIS evaluation of urban expansion and its impact on surface temperature in the Zhujiang Delta, China, *International Journal of Remote Sensing*, 22(10):1999–2014.

Xu, J., 1990. *A Collection of Essays on Lingnan Historical Geography* (Lingnan Lishi Dili Lunji), Zhongshan University Press (Zhongshan Daxue Xuebao Chubanshe), Guangzhou, China, 408 p. (in Chinese).

Yang, S., M. Zhang, and R. Zeng, 1984. The urban heat island effect of Guangzhou, *Journal of South China Normal University*, 1984(2):35–45 (in Chinese with English abstract).

(Received 12 October 2001; revised and accepted 10 September 2002)